Industrial Crops & Products 230 (2025) 121153

Contents lists available at ScienceDirect

Industrial Crops & Products

journal homepage: www.elsevier.com/locate/indcrop

Non-unified effects of cellulose allomorphs on fast pyrolysis and enzymatic hydrolysis

Hong-li Ma [a,b,c,1], Fei-xiang Xu [d,1], Ying-chuan Zhang [e], Miao-jun Huang [f], Ming-fu Li [b], Gui-hua Wang [b], Ming-xin Huang [b], Zhen Fang [a,*], Li-qun Jiang [b,*]

[a] Biomass Group, College of Engineering, Nanjing Agricultural University, Nanjing 210031, China
[b] Guangdong Engineering Laboratory of Biomass High-value Utilization, Institute of Biological and Medical Engineering, Guangdong Academy of Sciences, Guangzhou 510316, China
[c] College of Sciences, Nanjing Agricultural University, Nanjing 210095, China
[d] Inorganic Chemistry and Catalysis, Institute for Sustainable and Circular Chemistry, Utrecht University, Universiteitsweg 99, Utrecht, Netherlands
[e] Department of Chemistry, The University of Hong Kong, Hong Kong
[f] Yingde Zhi Shang Biomass Energy Technology Co., LTD., Qingyuan 513099, China

ARTICLE INFO

Keywords:
Biomass valorization
Saccharification
Fast Pyrolysis
Enzymatic hydrolysis
Levoglucosan
Bioethanol

ABSTRACT

Saccharification is a vital process to release sugar monomers from cellulose before the production of biofuels and fine chemicals. In this study, four distinct crystalline allomorphs of Cellulose (I–IV) are synthesized to examine the impact of crystalline structure and degree of crystallinity on cellulose depolymerization in pyrolysis and hydrolysis. It is found that cellulose with higher crystallinity produces higher yields of levoglucosan. Specifically, Cellulose II and III exhibit lower crystallinity index and levoglucosan yields compared to Cellulose I and IV. Notably, despite Cellulose IV having a higher crystallinity index than Cellulose I, the differences in crystalline structure and hydroxyl group level lead to a lower levoglucosan yield in pyrolysis. Thermogravimetric kinetics analysis suggests that cellulose with high crystallinity yields more anhydro-sugars through dehydration reactions, whereas amorphous cellulose predominantly produces lower molecular weight molecules through ring scission reactions. It is found that Cellulose II yields the maximum amount of glucose, while higher crystallinity levels have a negative impact on the sugar yield in general. This study provides a fundamental insight for modulating cellulose crystallinity towards effective utilization of biomass.

1. Introduction

Cellulose, a major component of lignocellulose, is a promising sustainable feedstock for large-scale energy production and the synthesis of high value-added chemicals (Verma et al., 2024). It is composed of long chains of β-D-glucan units connected by β-1,4-glycosidic bonds, with each unit having the chemical formula $(C_6H_{10}O_5)_n$. A complex network of hydrogen bonds, both within and between molecules, underpins the structure of cellulose, resulting in various crystalline forms (Cellulose I–IV). Natural cellulose exhibits a semi-crystalline nature, featuring both highly organized crystalline regions and less ordered amorphous regions. In the crystalline areas, cellulose organizes into microfibrils-structure formed by multiple β-1,4-D-glucan chains that are bonded through hydrogen bonds along their length, giving cellulose its characteristic rigidity and strength (Jarvis, 2023). The amorphous region is characterized by a lack of long-range order and a higher degree of orientation disorder among cellulose chains. Sugars are one of the key intermediates and saccharification represents a vital step in the transformation of cellulose through biological and chemical processes (Lv et al., 2022).

Commonly, enzymatic/acid hydrolysis is the most common approach to release glucose from cellulose (He et al., 2023; Xu et al., 2023). Cellulase or acids can effectively penetrate cellulose structure, break lignin-carbohydrate networks, and decrystallize cellulose, leading to the disruption of inter-chain hydrogen bonds and breakage of glycosidic bonds (Cheng et al., 2024). However, the challenges associated with handling acids and the difficulties in recycling them have restricted the widespread use of acid hydrolysis. Additionally, the

* Corresponding authors.
E-mail addresses: zhenfang@njau.edu.cn (Z. Fang), liqun_jiang2508@126.com (L.-q. Jiang).
[1] These authors contributed equally to this work

https://doi.org/10.1016/j.indcrop.2025.121153
Received 1 November 2024; Received in revised form 19 April 2025; Accepted 4 May 2025
Available online 8 May 2025

expenses related to pretreatment and enzyme usage pose significant barriers to the enzymatic hydrolysis process. The facility limitations and technical bottlenecks on the hydrolysis saccharification have been demonstrated to be complex and difficult to address (Wu et al., 2024a). While much of the focus has been on hydrolysis, levoglucosan production through fast pyrolysis emerges as an unavoidable alternative to release fermentable sugars from cellulose (Zhang et al., 2023). During fast pyrolysis, cellulose depolymerizes within several seconds without the utilization of catalysts or enzymes, leading to the dominant levoglucosan production. The maximum yield of levoglucosan from microcrystalline cellulose can achieve 70.1 wt%, while the concentration of levoglucosan is as high as 80 % in the pyrolytic syrup (Kwon et al., 2007). Due to its unique intramolecular ether bond, levoglucosan is a promising building block to produce pesticide, pharmaceuticals, and functional polymers endowed with specific stereochemistry. Biochemistry studies have proven that levoglucosan can be converted into glucose 6-phosphate through phosphorylation and subsequently metabolized via the glycolytic pathway into various chemicals, such as ethanol, lipids, malic acid, citric acid, and itaconic acid, with efficiency comparable to that of glucose (Jiang et al., 2019). Pyrolysis-derived sugar formation offers significant advantages over cellulose hydrolysis, including low cost of pretreatment and catalysts, fast rate of reaction and high concentrations of fermentable sugar. It has been proven that pyrolysis has economic benefits and reduced capital expenses in comparison to hydrolytic saccharification (Silveira Junior et al., 2022). Pyrolysis has the potential to open novel pathways that are not achievable through traditional hydrolysis reactions.

The yield of levoglucosan is influenced by the physical characteristics and purity of cellulose. In the fast pyrolysis of lignocellulose, the presence of inorganic impurities has been shown to alter chemical reaction pathways, leading to changes in the product distribution (Li et al., 2024). To improve the pyrolysis-derived sugar formation efficiency of lignocellulose, numerous efforts have been paid to pretreatment processes aimed at demineralization before fast pyrolysis (Li et al., 2024; Wu et al., 2024b). In contrast, the impacts of crystalline structure of cellulose, as a pivotal factor in pretreatment engineering of native biomass, has received less attention. Crystalline structure of cellulose could influence the pyrolysis behavior and product selectivity during thermal decomposition. Wang et al. reported that ball-milled cellulose with lower crystallinity produced less levoglucosan but more furans compared to high-crystallinity cellulose (Wang et al., 2013). Hosoya and Sakaki suggested that higher yields of levoglucosan could be obtained in the pyrolysis of cellulose with higher crystallinity (Hosoya and Sakaki, 2013). However, some previous studies have the opposite view. Kim et al. demonstrated that the crystal structure of cellulose had little effect on the activation energy required for its thermal decomposition (Kim et al., 2010). However, they found that as crystallite size increases, cellulose tends to degrade at higher temperatures. Zhang et al. observed that variations in crystallinity also had little impact on the types of pyrolysis products formed from cellulose (Zhang et al., 2014). Mukarakate et al. used theoretical models, including dimers and various oligomers, to study structural effects through computation (Mukarakate et al., 2016). Nonetheless, these models were significantly smaller than real cellulose, and the findings were not confirmed experimentally.

The structural features of cellulose could influence the pathways and rates of its fast pyrolysis, but no systematic investigation has been conducted. As a result, it is inadequate to determine how these structural characteristics affect the reaction mechanisms and the distribution of pyrolytic products. A thorough investigation is needed to clarify how the physical structural features of cellulose are related to the formation of levoglucosan. However, a comparative study on pyrolysis of cellulose with different crystalline structure and crystallinity, as a compensatory sector towards cost-effective fermentation and conversion of sugar monomer, has not been reported so far. Moreover, a detailed understanding of structural impacts is highly valuable and instructive to promote the production of levoglucosan. In this study, Cellulose I–IV are prepared and characterized, and the impact of crystalline structure on pyrolysis kinetics and product distribution is comprehensively investigated. Finally, a comparative analysis between fast pyrolysis and enzymatic saccharification to produce fermentable sugars from cellulose is provided. This investigation aims to offer essential insights into the mechanisms underlying cellulose pyrolysis and enhance the efficiency of the saccharification process. This study would also provide useful information to promote fermentable sugars production from biomass.

2. Materials and methods

2.1. Preparation of Cellulose I–IV

The crystalline allomorph Cellulose I (310697, Sigma-Aldrich) was purchased and utilized as the raw material to produce Cellulose II, III, and IV allomorphs. Cellulose I (cellulose I_β) was cotton fiber and Cellulose II was synthesized by dissolving Cellulose I (5 wt%) in aqueous NaOH solutions (18.5 wt%) for 1.5 h at 30℃, and the suspension was diluted in a beaker with distilled water. The sample was washed to a neutral pH and then freeze-dried (Gong et al., 2018). Cellulose III was synthesized by subjecting Cellulose I (5 wt%) to an anhydrous ethylenediamine solution for a duration 24 hours. Subsequently, the sample underwent multiple washings with anhydrous methanol to eliminate any residual ethylenediamine. The excess methanol was removed by an eyedropper and vacuum treatment was carried out at 30℃ to remove the residual methanol (Feng et al., 2020). Cellulose IV was prepared by immersing Cellulose III in glycerol for 3 days. The suspension was then heated at 260°C for 0.5 h. The precipitate was collected through filtration and subsequently rinsed with hot deionized water (Wada et al., 2004).

2.2. Structural characterizations

The functional groups of samples were examined using Fourier Transform Infrared Spectroscopy (FTIR) with a Bruker TENSOR27 instrument. Crystallinity index was determined by a X'Pert PROMPD X-ray diffract-meter (PANalytical V.B., Holland) , configured to operate at 40 kV and 40 mA. Each 80 mg sample underwent scanning across a diffraction angle (2θ) range of 5–45° with a step size of 0.01°, employing Cu radiation (λ=1.54 Å). Crystallinity index was computed using the following formula (Segal et al., 1959):

$$\text{Crystallinity index} = \frac{I_{002} - I_{am}}{I_{002}} \times 100\% \quad (1)$$

Here, I_{002} represents the highest peak intensity at $2\theta = 22.5°$, while I_{am} corresponds to the peak for the amorphous cellulose at $2\theta = 18°$.

The crystal size was determined using the Scherrer equation:

$$L_{002} = \frac{\kappa \times \lambda}{\beta_{hkl} \times \cos\theta} \times 100\% \quad (2)$$

Where β_{hkl} is the full width at half maximum of (002) peak, κ is Scherrer constant (0.94), θ is diffraction angle of (002) and λ is the wavelength of X-ray (λ=0.15406 nm) (Himmel et al., 2007).

Thermogravimetric analysis was conducted using a TG system (209 F3 Tarsus). Each cellulosic sample was subjected to heating from 30 to 700°C at different heating rates (10–60 °C/min) under nitrogen atmosphere (20 mL/min). D_{max} and T_{max} refer to the mass loss and temperature at the peak of the derivative DTG analysis, T_i is the initial temperature of primary mass loss region, where a 5 % weight loss is observed and T_t is the terminal temperature of this region, corresponding to an 80 % weight loss.

2.3. Kinetic analysis

The distributed activation energy model (DAEM) is frequently uti-

lized to analyze the kinetics of the cellulose pyrolysis. This model assumes the thermal decomposition of cellulose consisted of a multitude of independent, parallel, and first-order reactions. The activation energy of these reactions can be represented by Gaussian distribution (f(E)~N(E, σ)). The basic non-isothermal heterogeneous equation can be described by the Arrhenius law:

$$\frac{d\alpha}{dt} = A\exp\left(\frac{-E}{RT}\right)f(\alpha) \tag{3}$$

Where α is the conversion rate of cellulose, t is the reaction time, E is the activation energy, A is the frequency factor, R is the universal gas constant, and T is the reaction temperature.

By considering β=dT/dt. The Eq. (4) can be obtained.

$$\frac{d\alpha}{f(\alpha)} = \frac{A}{\beta}\exp\left(\frac{-E}{RT}\right)dT \tag{4}$$

The first order reaction mechanism is usually used in DAEM, leading to Eq. (5):

$$-\ln(1-\alpha) = \frac{A}{\beta}\int_0^T \exp\left(\frac{-E}{RT}\right)dT \tag{5}$$

Finally, the function of the conversion rate can be expressed as Eq. (6):

$$\alpha = 1 - \exp\left(-\frac{A}{\beta}\Psi(E,T)\right) \tag{6}$$

Where $\Psi(E,T) \sim \int_0^T \exp\left(\frac{-E}{RT}\right)dT$.

Thus, the equation for DAEM can be expressed as (7):

$$\alpha = 1 - \int_0^\infty \exp\left(-\frac{A}{\beta}\Psi(E,T)\right)f(E)dE \tag{7}$$

By setting the frequency factor as a constant, the other kinetic triplets (activation energy and reaction mechanism) can be solved through numeral calculation and optimal algorithm.

2.4. Fast pyrolysis

Cellulose pyrolysis was performed in a pyroprobe (EGA/PY-3030D, Frontier, Japan) connected to a GC/MS system (7890 A/5975 C, Agilent Technologies, USA). The temperature of cracker was heated from 50°C to 500°C at a rate of 10°C/ms and maintained at 500°C for 20 s. High-purity helium was employed at a flow rate of 20 mL/min to transport the pyrolyzed volatiles through a transmission line maintained at 300°C into the GC-MS system for product separation and identification. Separation was achieved using a VT-1701MS capillary column with a 100:1 split ratio. The GC oven was initially set at 40°C for 3 min, then ramped to 280°C at a rate of 5 °C/min and maintained at this temperature for 8 min. The mass spectrometry parameters included an ion source temperature of 230°C, a quadrupole temperature of 150°C, ion source energy of 70 eV, and a scan range (*m/z*) of 29–450 amu. The yield of levoglucosan and relative content of compounds were computed as follows:

$$\text{Levoglucosan yield (wt\%)} = \frac{\text{Mass of levoglucosan}}{\text{Mass of cellulose}} \times 100\% \tag{8}$$

$$\text{Relative content of compound(\%)} = \frac{\text{Area of a compound}}{\text{Area of all compounds}} \times 100\% \tag{9}$$

2.5. Enzymatic hydrolysis

A 50-mL Erlenmeyer flask was utilized for enzymatic hydrolysis, which took place in a shaker for 12 h, with a sodium citrate reaction buffer (50 mM, pH 4.8) maintained at 50°C. Enzymatic hydrolysis involved a cellulose concentration of 10 % w/v, accompanied by a cellulase activity of 20 FPU/g cellulose. The enzymatic activity of cellulase (Sigma-aldrich C2730, Denmark) was analyzed by the method of NREL. To prevent microbial growth, 2 % sodium azide was added. During hydrolysis, the supernatant was analyzed using high performance liquid chromatography (HPLC) (Agilent 1260 infinity II, Agilent Technologies, USA). Dilute H_2SO_4 (0.005 mol/L) was used as the mobile phase and the flow rate was set at 0.5 mL/min. The content of glucose was separated by an HPX-87H column (Bio-Rad, U.S.) at 65°C and determined by a refractive index detector at 50°C. The yield of glucose was determined as follows:

$$\text{Glucose yield (wt\%)} = \frac{\text{mass of glucose}}{\text{mass of cellulose}} \times 0.9 \times 100\% \tag{10}$$

Where 0.9 is the glucose to cellulose conversion factor.

3. Results and discussion

3.1. Surface and crystallinity analysis

The SEM plots of four cellulose samples are illustrated in Fig. 1. In comparison to Cellulose I, the structures of Cellulose II, III, and IV change remarkedly. The surface of cellulose I appears relatively smooth and compact. Cellulose II displays a fibrous and layered appearance. Cellulose III shows a corrugated surface appearance, and Cellulose IV displays a relatively smooth and compact structure. The XRD analysis of cellulose is exhibited in Fig. 2(a). Cellulose I exhibits characteristic diffraction peaks at 2θ = 14.7°, 15.6°, and 22.5°, which are linked to the (1–10), (110), and (200) crystallographic planes, respectively (Liu et al., 2022). Cellulose II displays a new diffraction peak at 2θ = 12.1°, which is associated with the (1–10) plane. Additionally, the peaks at 2θ = 20°–22° overlap, but two peaks corresponding to the (110) and (020) planes can still be observed near 2θ = 20.1° and 21.8°. The absence of characteristic peaks of Cellulose I indicates its complete transformation into Cellulose II (French, 2014; Gong et al., 2018; Zhang et al., 2014). When Cellulose I is treated with ethylenediamine, the diffraction pattern of Cellulose III changes significantly. The peak for Cellulose I shifts from 2θ = 22.5° to 2θ = 20.9°, corresponding to the overlapping peaks in the (110), (012), and (1–10) planes, indicating a change from Cellulose I to III (Chundawat et al., 2011; French, 2014). For crystal plane [110] stack, parallel cellulose I and antiparallel cellulose II were shifted, but there is no stagger of the cellulose III chains (Yoneda et al., 2008). Characteristic peaks of Cellulose III appear at 2θ= 11.8° and 17.2°, related to the (010) and (002) planes, respectively. Further high-temperature treatment of Cellulose III leads to the disappearance of the peaks at 2θ= 11.8° and 20.9°, with new peaks at 2θ= 15.5° and 22.4° emerging, which are associated with the (1–10), (110), and (200) planes, indicating the transformation of Cellulose III into IV (Huang et al., 2022). The crystallinity index and crystal size of cellulose samples are presented in Table 1. The crystallinity index of cellulose represents the proportion of crystalline regions within the cellulose structure, indicating the extent to which cellulose is arranged in a highly ordered, repeating pattern. Crystal size, on the other hand, refers to the size of these crystalline regions within the cellulose matrix. Different cellulose allomorphs exhibit distinct crystalline structures and sizes, influenced by both intrinsic factors (such as cellulose source and crystallinity index) and extrinsic factors (such as experimental methods). As shown in Table 1, the order of crystallinity among the cellulose allomorphs is as follows: Cellulose III < II < I < IV. For crystal size, the order is: Cellulose IV < II < I < III. This implies that a clear connection between crystallinity and crystal size is absent. Notably, among the cellulose allomorphs, Cellulose III exhibits the lowest crystallinity index while possessing the largest crystal size. This suggests that although Cellulose III has a lower frequency of crystalline regions, these regions are more extended compared to those in other cellulose forms.

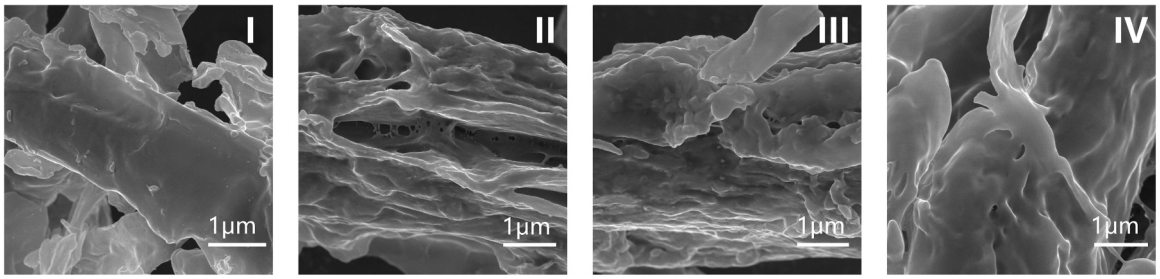

Fig. 1. SEM pattern of Cellulose I-IV.

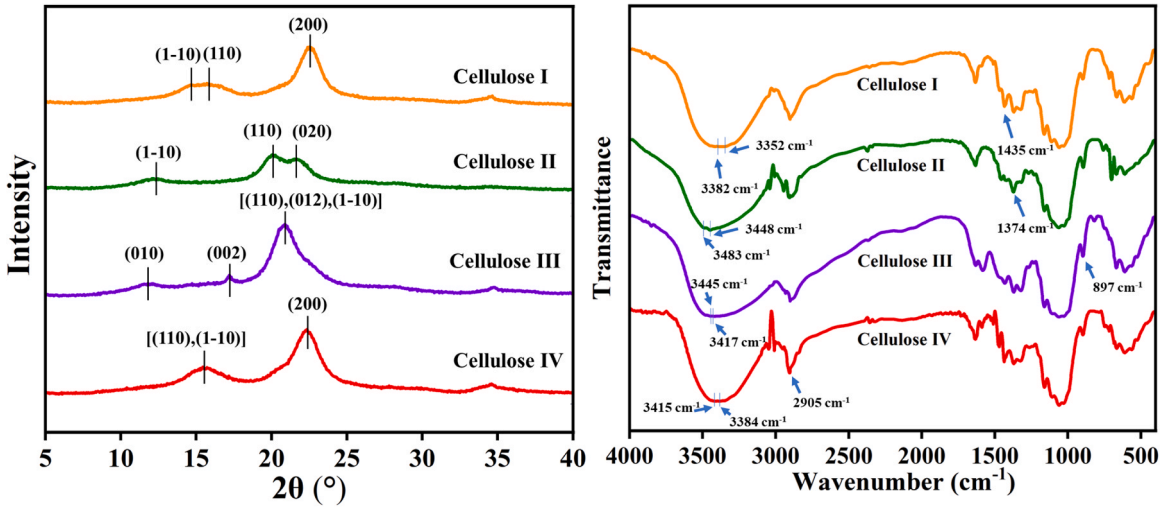

Fig. 2. XRD and FTIR spectra of Cellulose I-IV.

Table 1
Structural and thermal characteristic parameters of Cellulose I-IV.

Samples	Crystallinity index (%)	Crystal size (nm)	Heating rate (℃/min)	T_i (℃)	T_t (℃)	T_{max} (℃)	D_{max} (%)
Cellulose I	75.9	4.6	20	328.1	379.1	354.7	2.4
			30	335.6	387.2	363.1	2.4
			40	341.0	392.7	368.1	2.3
			60	348.8	402.6	375.3	2.2
Cellulose II	72.8	4.1	20	323.8	378.9	354.6	2.2
			30	332.1	387.1	362.6	2.1
			40	337.5	393.3	366.4	2.1
			60	344.1	403.1	375.9	2.0
Cellulose III	69.3	7.2	20	332.8	383.3	359.1	2.2
			30	339.9	390.3	366.0	2.2
			40	345.1	395.9	372.2	2.1
			60	352.2	406.3	381.6	2.0
Cellulose IV	78.2	3.1	20	323.9	378.9	354.6	2.2
			30	332.1	386.8	362.6	2.1
			40	337.2	393.3	366.4	2.1
			60	343.2	402.7	376.0	2.0

3.2. FTIR analysis

The FTIR spectra of the four cellulose samples are shown in Fig. 2(b). The FTIR results suggest that the structural integrity of cellulose was preserved within the four samples, indicating similar chemical structures. In all samples, the bands appearing between 3400 and 3300 cm^{-1} are attributed to the stretching vibrations of the hydroxyl groups (OH), indicating the presence of side chains (–CH–OH) and (–CH_2–OH) in cellulose. Another prominent vibration between 3000 and 2800 cm^{-1}corresponds to C–H stretching. Given that the ratio of CH to CH_2 in cellulose is 5:1, this band is primarily assigned to the CH groups (Silva Filho et al., 2013). The peak at 1640 cm^{-1} in all samples is due to the deformation vibration of primary and secondary hydroxyl groups, signifying water absorption. The peak between 1200 and 1000 cm^{-1}refers to the stretching vibration of C–O–C, indicating the pyranose ring skeletal structure (Park et al., 2024). The peak at 894 cm^{-1}characterizes the β-1,4-glycosidic bond vibration (Atykyan et al., 2020).

The main difference between the FTIR curves of Cellulose I and II is the strong absorption in the O–H stretching vibration region. Generally, the wavenumber of the O–H stretching in Cellulose II is higher than in Cellulose I, indicating a blue shift (Yue et al., 2015). This suggests that the hydrogen bonds in Cellulose II are stronger than in Cellulose I, and the reverse parallel arrangement of Cellulose II results in a smaller polar

structure. This increases the stretching frequency of free O–H, enhancing the stability and activation energy of Cellulose II (Table 3). The O–H stretching vibration occurs at 3416 cm^{-1}in Cellulose I and at 3448 cm^{-1}in Cellulose II. The infrared spectra of Cellulose III and IV are very similar to those of Cellulose I and II, except for a peak at 1575 cm^{-1} , which corresponds to the N–H deformation in primary amines (Bezerra et al., 2017).

3.3. TG analysis

To better understand the pyrolysis characteristics of cellulose exhibiting various crystalline configurations, the TG (thermogravimetric) and DTG (derivative thermogravimetric) curves for cellulose pyrolysis at heating rates of 20, 30, 40, and 60 °C/min are shown in Fig. 3. At low temperatures (< 105°C), the initial small weight loss in all samples corresponds to the evaporation of absorbed water. It has been reported the effects of particle size, sweep gas flow rates, and cellulose masses on pyrolysis behavior, showing that the initial cellulose mass significantly impacts the pyrolysis behavior (Lin et al., 2009). Additionally, the crystalline structure of cellulose influences its pyrolysis behavior, though this area has been less extensively studied. The TG characteristic parameters are shown in Table 1. The initial pyrolysis temperatures of cellulose types are ordered as follows: Cellulose III > I > II ≈ IV. At a heating rate of 60 °C/min, the maximum degradation temperatures for Cellulose I–IV are 375.3°C, 375.9°C, 381.6°C, and 376.0°C, respectively, with all degradation completed at around 380 °C. This indicates that despite changes in polycrystalline form, all cellulose samples exhibit similar thermal degradation behavior (Gong et al., 2018; Li et al., 2022). Cellulose III has the highest degradation temperature due to the presence of more hydrogen bonds between Cellulose III chains, leading to a more packed structure, higher crystallinity, and greater thermal stability (de Souza et al., 2020). This result is also supported by the following kinetic analysis.

The main pyrolysis region for all four celluloses with different crystalline structures is located between 300 and 400°C. According to the TG data, there are slight differences between the different cellulose allomorphs. The apparent activation energy is sensitive to changes in the TG curves for different samples (Yang et al., 2018). Heating rate is a key factor in cellulose pyrolysis, with the onset and offset temperatures of the main weight loss stage shifting to a higher temperature range as the heating rate increases (Fig. 3). Additionally, the DTG peak at a higher heating rate is lower than that at a lower heating rate, a phenomenon caused by heat and mass transfer limitations (Chen et al., 2014). The low thermal conductivity of the polymer leads to a thermal gradient, which is caused by structural defects, which encompass amorphous regions, voids, chain ends, and entanglements (Uetani and Hatori, 2017). All samples show only one weight loss peak during pyrolysis in the DTG (Fig. 3), corresponding to the depolymerization of cellulose, which is the rate-determining reaction. From the DTG data, it is evident that the rate-determining reaction of cellulose pyrolysis does not change with different crystalline structures.

3.4. Kinetic analysis

TG is a valuable tool for directly observing the thermal behavior of solid samples. Thermal kinetics can provide deep insights into thermal behavior such as reaction rates and activation energy. By analyzing the kinetics triplet, a detailed pyrolysis profile can be elucidated. The DAEM has been widely recognized as an effective tool for analyzing the relationship between kinetic triplets, activation energy, frequency factor, and reaction mechanism. In the DAEM, the frequency is usually set as a constant, meaning that changes in activation energy depend solely on the reaction mechanism. The DAEM kinetic parameters for different heating rates and those for different frequency factors are shown in Table 2 and Table 3. The correction coefficient R^2 value for all samples is higher than 0.99, demonstrating the accuracy of the DAEM for this study. The activation energy shows a compensation relationship with

Table 2
Thermal kinetics of Cellulose I-IV.

Samples	β (K/min)	lgA	E (kJ/mol)	σ (kJ/mol)	R^2
Cellulose I	20	20	235.5	4.3	0.9991
	30	20	236.3	4.3	0.9990
	40	20	237.1	4.6	0.9991
	60	20	239.1	5.3	0.9996
Cellulose II	20	20	239.3	0.2	0.9994
	30	20	241.1	0.2	0.9994
	40	20	241.2	0.5	0.9995
	60	20	242.6	1.7	0.9998
Cellulose III	20	20	242.5	0.4	0.9979
	30	20	243.3	0.3	0.9981
	40	20	244.0	0.2	0.9982
	60	20	244.9	0.2	0.9985
Cellulose IV	20	20	240.9	0.2	0.9974
	30	20	241.4	0.2	0.9975
	40	20	243.0	0.3	0.9974
	60	20	244.4	0.1	0.9983

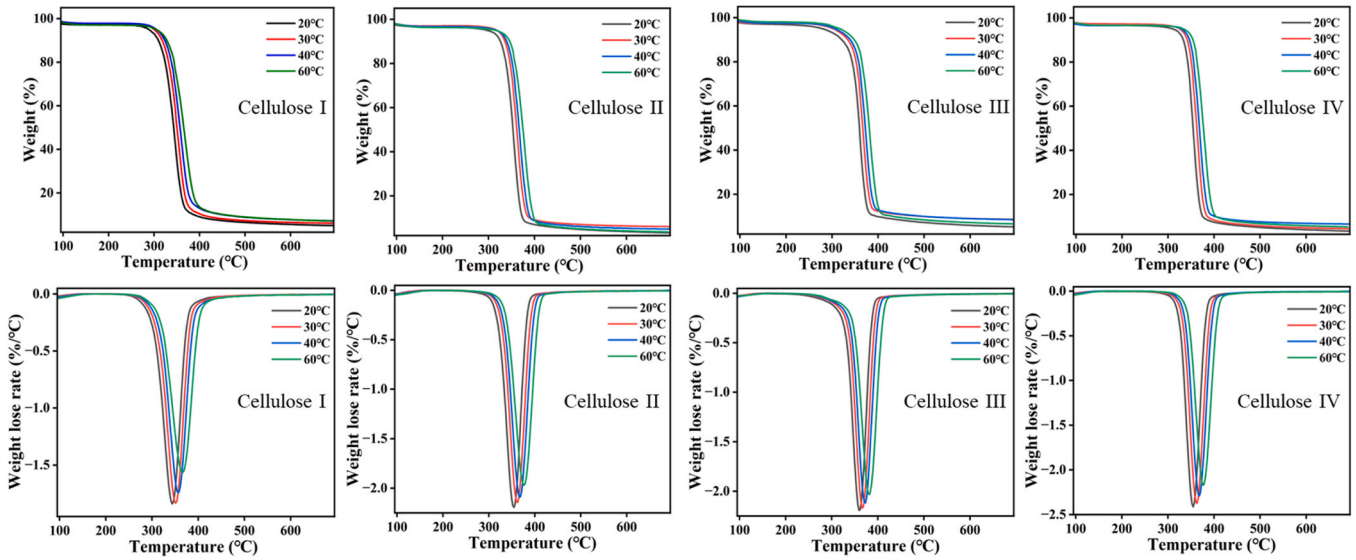

Fig. 3. TG and DTG pattern of Cellulose I-IV.

Table 3
DAEM parameters of Cellulose I-IV based on 60 K/min.

lgA	Samples	E (kJ/mol)	σ (kJ/mol)	R^2
20	Cellulose I	239.1	5.3	0.9996
	Cellulose II	242.6	1.7	0.9998
	Cellulose III	244.9	0.2	0.9985
	Cellulose IV	244.4	0.1	0.9983
25	Cellulose I	299.2	7.9	0.9993
	Cellulose II	303.6	4.7	0.9998
	Cellulose III	306.5	4.2	0.9978
	Cellulose IV	306.0	2.8	0.9996
30	Cellulose I	359.5	10.4	0.9992
	Cellulose II	364.7	6.8	0.9996
	Cellulose III	368.3	6.5	0.9972
	Cellulose IV	367.6	5.0	0.9998
35	Cellulose I	419.8	12.7	0.9991
	Cellulose II	426.0	8.8	0.9995
	Cellulose III	430.1	8.5	0.9968
	Cellulose IV	429.4	6.8	0.9998
	Cellulose I	$E = 12.046lgA - 1.834$; $R^2 = 1$		
	Cellulose II	$E = 12.23lgA - 2.113$; $R^2 = 1$		
	Cellulose III	$E = 12.351lgA - 2.221$; $R^2 = 1$		
	Cellulose IV	$E = 12.3331lgA - 2.3$; $R^2 = 1$		

lg*A*, with a correction coefficient of 1, further proving the accuracy of the DAEM. The pyrolysis behavior of cellulose depends on its characteristics, such as degree of depolymerization, crystallinity index, and crystal size (Eugenio et al., 2021). The crystalline structures of Cellulose I-IV differ, resulting in different kinetics parameters. For a constant frequency factor and heating rate, the activation energy E is ordered as follows: Cellulose III≈IV > II > I. The order of σ was Cellulose I > II > III > IV. Activation energy reflects the rate of the pyrolysis reaction, and higher activation energy means that reactant requires more energy to reach the transition state, thus decreasing the reaction rate. The highly ordered crystal structure of Cellulose I results in hydrogen bonds between molecular chains being arranged regularly and in a consistent direction. This regular arrangement reduces the number of hydrogen bonds that need to be disrupted during the early stages of pyrolysis. Despite having a large number of hydrogen bonds, the synergistic effects within this network facilitate a reaction pathway that favors direct dehydration reactions, such as the formation of levoglucosan, rather than more energy-demanding chain breakage or ring cleavage reactions. Consequently, this pathway requires less activation energy. While Cellulose IV also features an ordered hydrogen bonding scheme similar to Cellulose I, it contains additional hydrogen bonds within each of the two intrasheets of the crystal cell. These additional hydrogen bonds increase the activation energy required for pyrolysis. The change in activation energy observed for cellulose allomorphs indicated a shift in the pyrolysis reaction mechanism. σ indicates the activation energy distribution, where higher σ values represent a broader distribution. This also reflects the crystalline structure of cellulose. The molecular chains in the crystalline regions of higher crystallinity cellulose are more orderly and compact, leading to more intense thermal decomposition.

The DAEM curves with different heating rates and frequency factors are shown in Fig. 4 and Fig. 5. Activation energy reflects the reaction rates, while the reaction mechanism highlights the physical and geometrical characteristics of the reaction. These features primarily include the initial reaction sites being spatially constrained, along with the geometrically restricted advancement of the reaction interface in the later stages of reaction (Koga et al., 2023). By analyzing these physico-geometrical features, a detailed pyrolysis behavior model can be developed. Given that cellulose consists of linear β-1,4-glycosidic bond, the DAEM fits well with the main decomposition stage of cellulose. However, there are two deviations observed in the conversion curve. The first deviation occurs at a lower temperature (~350℃), which marks the onset of the rate-determining reaction. This deviation is more pronounced in Cellulose III and IV, indicating that the initial reaction stage in these forms of cellulose differs from that in Cellulose I and II. The second deviation occurs at the end of the pyrolysis stage in all samples, which is typically regarded as the end of the main pyrolysis

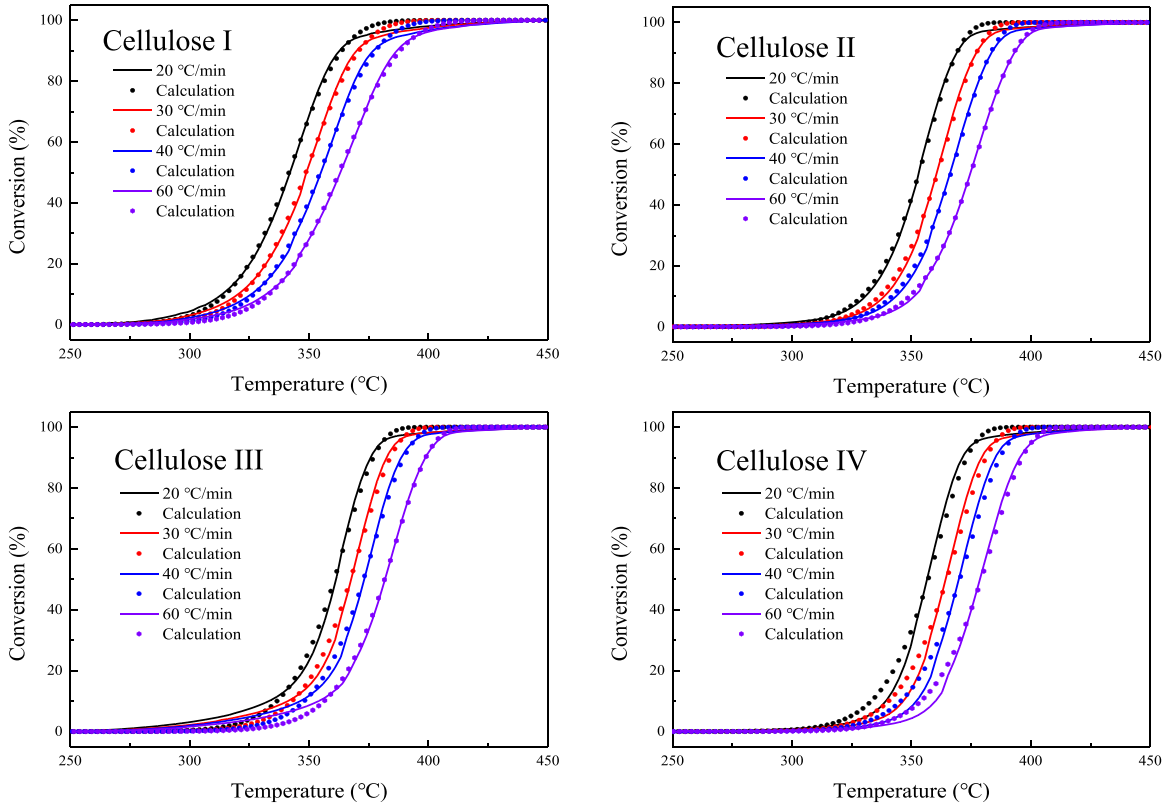

Fig. 4. DAEM curves for different heating rates of Cellulose I-IV.

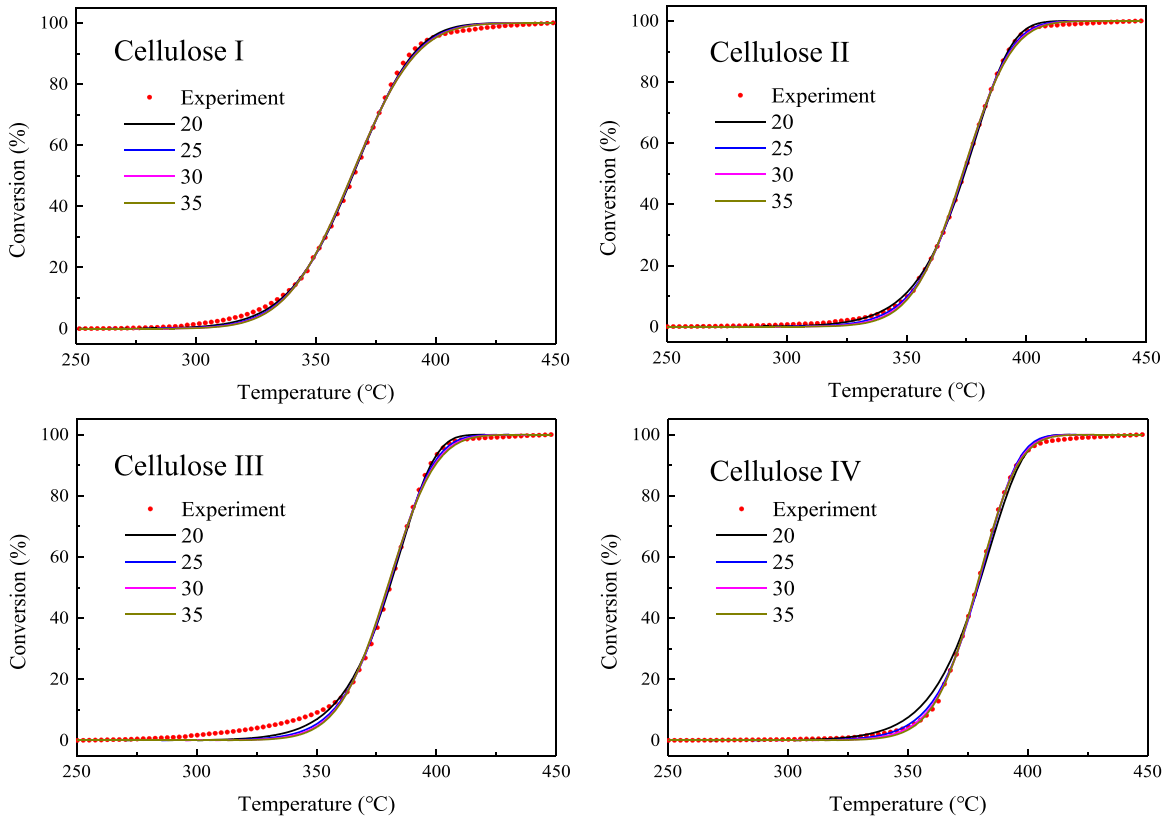

Fig. 5. DAEM curves for different frequency factors.

decomposition, and the end of the rate-determining reaction. After this stage, cellulose undergoes carbonization to form char instead of oxygenates.

3.5. Fast pyrolysis

The relative content of pyrolysis products and yield of levoglucosan from cellulose are presented in Table 4 and Fig. 6(a). When cellulose underwent pyrolysis at 400 ℃, it predominantly produces anhydrosugars like levoglucosan and 1,6-anhydro-β-D-glucofuranose, with an anhydro-sugar relative content reaching up to 92.3 % (Table 4). However, as the crystallinity of cellulose decreases, the relative content of anhydro-sugars also diminishes. This decrease in crystallinity correlates with an increase in the yield of lower molecule weight compounds, suggesting that the changes in crystallinity and crystalline structure promote ring scission reactions (to produce small-molecule oxygenates) over dehydration reactions (to produce anhydrosugars). This shift in reaction pathways also corresponds with the observed increase in apparent activation energy calculated from DAEM (Table 3). The order of levoglucosan yield is as follows: Cellulose I > IV > II > III. This trend demonstrates that the crystalline structure significantly influences the yield of levoglucosan during cellulose pyrolysis. The strength and arrangement of the hydrogen bond network can affect the dehydration efficiency of cyclic sugar molecules. Among four cellulose samples, Cellulose I with stronger hydrogen bonds is more conducive to dehydration reactions, achieving the highest levoglucosan yield (50 wt%) at 400°C. When the crystallinity index decreases from 76 % to 69 %, the levoglucosan yield drops from 50 wt% to 28 wt%. Despite the crystallinity index of Cellulose IV increasing to 78 %, its levoglucosan yield (40 wt%) is lower than that of Cellulose I. The partial depolymerization of Cellulose IV during thermal pretreatment results in a decreased levoglucosan yield.

Considering that the chemical structure of the different cellulose samples did not change, it can be concluded that the differences in apparent activation energy and pyrolysis product distribution among the four cellulose samples are attributable to changes in their crystalline structures. Different cellulose crystal structures possess unique hydrogen bonding networks (Wohlert et al., 2022), which play a crucial role in determining the reaction pathways and product distribution during pyrolysis. The highly ordered structures and robust hydrogen-bonded networks in Cellulose I and IV tend to favor cohesive, direct dehydration reactions, leading to higher selectivity for anhydrosugars. In contrast, Cellulose II and III feature weaker or irregular hydrogen bonds, making them more prone to breakage and resulting in the formation of more small-molecule oxidized products. Despite Cellulose IV having the highest crystallinity, its levoglucosan yield is lower than that of Cellulose I, primarily due to chain depolymerization and hydrogen bond disruption from thermal pretreatment. This suggests that even with high crystallinity, the distribution of pyrolysis products can change significantly if the hydrogen bond network has been destroyed or modified (*e.g.,* by thermal pretreatment).

3.6. Enzymatic hydrolysis

In comparison, the enzymatic hydrolysis of different cellulose allomorphs has also been explored. A comprehensive investigation has been conducted on how crystalline structure affects the hydrolysis of cellulose, and a negative correspondence is found between the crystallinity and the hydrolysis rate. This arises from the configuration of β-1,4-glycosidic bonds and the hydrogen bonds between glucose units, which inhibit the approaching of water molecules to break these bonds (Harada et al., 2014). In this study, Cellulose IV exhibits the fastest reaction before 6 h hydrolysis, while Cellulose II gave the highest glucose yield (29.4 wt%) and Cellulose III showed the lowest (18.7 wt%) after 12 h hydrolysis presented in Fig. 6(b). Cellulose II undergoes faster depolymerization than Cellulose I and II showing a positive impact in

Table 4
The pyrolysis product distribution of Cellulose I-IV.

Time (min)	Compound	Selectivity (%)							
		500 ℃				400 ℃			
		Cellulose I	Cellulose II	Cellulose III	Cellulose IV	Cellulose I	Cellulose II	Cellulose III	Cellulose IV
1.3	Ethylene oxide	2.2	3.0	4.2	2.4	0.5	3.0	8.1	7.6
1.9	Methyl glyoxal	0.7	1.6	1.8	1.3	0.0	0.0	0.0	0.0
3.1	Acetaldehyde, hydroxy-	1.2	6.4	6.2	3.0	0.0	0.0	0.0	0.0
9.1	Propanoic acid, 2-oxo-, methyl ester	0.0	0.0	0.5	0.0	0.0	0.0	0.0	0.0
9.4	Furfural	0.3	0.8	0.8	0.6	0.0	0.0	0.0	0.0
12.7	Cyclobutanol	0.2	0.0	0.0	0.3	0.0	0.0	0.0	0.0
12.9	2-Cyclopenten−1-one, 2-hydroxy-	0.0	0.7	1.0	0.5	0.0	0.8	1.2	0.0
15.1	2,4(1H,3H)-Pyrimidinedione, dihydro-	0.0	0.0	0.8	0.5	0.0	0.0	0.0	0.0
15.6	Dihydroxyacetone	0.0	0.8	0.7	0.0	0.0	0.8	0.8	0.0
19.9	Levoglucosenone	0.3	0.0	0.0	0.0	1.0	0.0	0.0	0.0
22.4	Heptanal	0.5	1.8	1.1	1.2	0.5	1.3	1.0	0.8
23.3	1,4:3,6-Dianhydro-.alpha.-d-glucopyranose	0.3	0.0	0.0	0.0	0.0	0.0	0.0	0.0
25.1	5-Hydroxymethylfurfural	0.4	2.2	2.9	1.7	0.0	2.7	3.6	1.5
26.6	1,3-Dioxolane, 2-ethyl−4-methyl-	2.3	7.4	8.2	0.0	2.8	0.0	0.0	0.0
33.3	Levoglucosan	80.1	68.9	65.1	75.1	83.7	77.3	71.0	76.7
35.5	3,4-Dimethylpentanoic acid	0.0	1.8	2.2	1.8	1.7	0.7	2.5	1.9
36.4	1,6-Anhydro-.beta.-D-glucofuranose	7.3	2.9	2.2	4.1	8.6	4.6	3.0	4.9

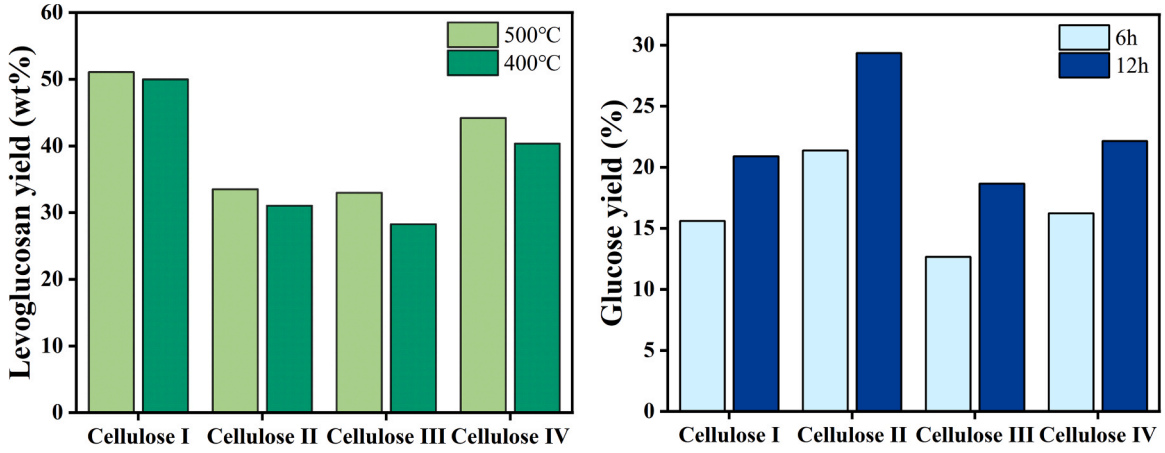

Fig. 6. Levoglucosan and glucose yields of Cellulose I-IV.

enzymatic hydrolysis, attributed to weaker hydrophobic interactions within cellulose chains (Sang et al., 2022). This phenomenon can be attributed to a greater number of available channels on the crystalline surfaces and the swollen cellulose surface increases the surface area and promotes the accessibility of enzymes. Besides crystallinity, the changes in OH groups may also play a significant role in cellulose hydrolysis. Comparing Cellulose II and III reveals that the influence of OH groups or crystalline structure on cellulose hydrolysis is more pronounced than that of crystallinity. The more open structure of Cellulose II enhances enzyme access, whereas the tightly packed structure of Cellulose III limits hydrolytic efficiency.

Until recently, it has rarely been reported a systematic comparison between enzymatic hydrolysis and pyrolysis-derived sugar formation. It is crucial to assess both the advantages and weaknesses of each method when selecting available raw material and energy-effective technologies. Enzymatic hydrolysis offers benefits including mild operating condition, high selectivity, and low toxicity. However, it also demands expensive pretreatment and cellulase to address cellulose's structural barriers. In contrast, fast pyrolysis provides higher efficiency and greater sugar concentrations. Notably, enzymatic hydrolysis can achieve a

glucose yield of up to 67 %, the glucose content was relatively low (~1 %) compared to the high concentration of levoglucosan (~80 %) found in pyrolysis products. High concentrations of sugar are beneficial for obtaining high concentrations of products, thus reducing the expenses associated with product separation. Economic analyses suggest that integrating pyrolysis-derived sugar formation is economically viable and comparable to enzymatic hydrolysis and fermentation (So and Brown, 1999). Undoubtedly, fermentable levoglucosan production by fast pyrolysis has the potential for further development. After understanding the discrepancy in cellulose allomorphs features during fast pyrolysis and enzymatic hydrolysis, it is beneficial to design process integrating pretreatment, saccharification and downstream fermentation towards effective fermentable utilizations of cellulose.

4. Conclusions

A comparative investigation was performed for fermentable sugars production from cellulose by fast pyrolysis and enzymatic hydrolysis. The impacts of crystallinity and the re-arrangement of crystalline structures on pyrolysis and hydrolysis of cellulose allomorphs (I–IV) were investigated by kinetic analysis and product profiling. The effects of crystalline structures on pyrolysis and hydrolysis were found to be significantly distinguished in terms of the efficiency and selectivity in producing sugar monomers. In pyrolysis, the crystalline structure positively influenced the yield of levoglucosan, and Cellulose I achieved the highest levoglucosan yield. In contrast, amorphous cellulose would produce small-molecule oxygenates via ring scission reactions with a remarkably increased apparent activation energy. In hydrolysis, however, the crystalline structure exhibited a negative effect on the sugar yield, with Cellulose II yielding the maximum amount of glucose.

CRediT authorship contribution statement

Hong-li Ma: Data curation, Methodology, Formal analysis, Investigation, Writing – original draft. **Fei-xiang Xu:** Data curation, Methodology, Formal analysis, Investigation, Writing – original draft. **Yingchuan Zhang:** Formal analysis, Writing – original draft. **Miao-jun Huang:** Data curation, Methodology, Formal analysis. **Gui-hua Wang:** Formal analysis, Writing – original draft. **Ming-xin Huang:** Formal analysis. **Li-qun Jiang:** Conceptualization, Supervision, Funding acquisition, Writing – review & editing. **Zhen Fang:** Conceptualization, Supervision, Writing – review & editing.

Declaration of Competing Interest

The authors declare that they have no known competing financial interests or personal relationships that could have appeared to influence the work reported in this paper.

Acknowledgements

This work was supported by GDAS' Project of Science and Technology Development (2022GDASZH-2022010110, 2023GDASZH-2023010102).

Data availability

Data will be made available on request.

References

Atykyan, N., Revin, V., Shutova, V., 2020. Raman and FT-IR spectroscopy investigation the cellulose structural differences from bacteria gluconacetobacter sucrofermentans during the different regimes of cultivation on a molasses media. AMB Express 10, 84. https://doi.org/10.1186/s13568-020-01020-8.

Bezerra, R.D.S., Leal, R.C., da Silva, M.S., Morais, A.I.S., H. C. Marques, T., A. Osajima, J., B. Meneguin, A., Da S. Barud, H., C. da Silva Filho, E., 2017. Direct modification of microcrystalline cellulose with ethylenediamine for use as adsorbent for removal amitriptyline drug from environment. Molecules 22, 2039. https://doi.org/10.3390/molecules22112039.

Chen, D., Zhou, J., Zhang, Q., 2014. Effects of heating rate on slow pyrolysis behavior, kinetic parameters and products properties of moso bamboo. Bioresour. Technol. 169, 313–319. https://doi.org/10.1016/j.biortech.2014.07.009.

Cheng, X., Feng, C., Li, Z., Zhang, W., Ji, L., Wang, K., Jiang, J., 2024. Efficient and comprehensive utilization of sugarcane bagasse components through vanillic acid pretreatment. Chem. Eng. J. 493, 152719. https://doi.org/10.1016/j.cej.2024.152719.

Chundawat, S.P.S., Bellesia, G., Uppugundla, N., da Costa Sousa, L., Gao, D., Cheh, A.M., Agarwal, U.P., Bianchetti, C.M., Phillips Jr., G.N., Langan, P., Balan, V., Gnanakaran, S., Dale, B.E., 2011. Restructuring the crystalline cellulose hydrogen bond network enhances its depolymerization rate. J. Am. Chem. Soc. 133, 11163–11174. https://doi.org/10.1021/ja2011115.

Eugenio, M.E., R, M., M, R., Ibarra, D., Díaz, M.J., 2021. Influence of cellulose characteristics on pyrolysis suitability. Processes 9, 1584. https://doi.org/10.3390/pr9091584.

Feng, L., Ling, Z., Ma, J., Liu, X., Jiang, Z., 2020. Recrystallization behavior of cellulose III from hydrothermal treatment: the dynamic variations of polymorphs and crystallinities. Wood Sci. Technol. 54, 1605–1616. https://doi.org/10.1007/s00226-020-01220-2.

French, A.D., 2014. Idealized powder diffraction patterns for cellulose polymorphs. Cellulose 21, 885–896. https://doi.org/10.1007/s10570-013-0030-4.

Gong, J., Mo, L., Li, J., 2018. A comparative study on the preparation and characterization of cellulose nanocrystals with various polymorphs. Carbohydr. Polym. 195, 18–28. https://doi.org/10.1016/j.carbpol.2018.04.039.

Harada, T., Tokai, Y., Kimura, A., Ikeda, S., Matsumura, M., 2014. Hydrolysis of crystalline cellulose to glucose in an autoclave containing both gaseous and liquid water. RSC Adv. 4, 26838–26842. https://doi.org/10.1039/C4RA02396J.

He, B., Yu, Y., Gong, X., Liu, S., Tian, H., Leng, E., 2023. Mechanism of acid-catalyzed pyrolysis of levoglucosan: formation of anhydro-disaccharides. Fuel 345, 128242. https://doi.org/10.1016/j.fuel.2023.128242.

Himmel, M.E., Ding, S.Y., Johnson, D.K., Adney, W.S., Nimlos, M.R., Brady, J.W., Foust, T.D., 2007. Biomass recalcitrance: engineering plants and enzymes for biofuels production. Science 315, 804–807. https://doi.org/10.1126/science.1137016.

Hosoya, T., Sakaki, S., 2013. Levoglucosan formation from crystalline cellulose: importance of a hydrogen bonding network in the reaction. ChemSusChem 6, 2356–2368. https://doi.org/10.1002/cssc.201300338.

Huang, C., Yu, H., Abdalkarim, S.Y.H., Li, Y., Chen, X., Yang, X., Zhou, Y., Zhang, L., 2022. A comprehensive investigation on cellulose nanocrystals with different crystal structures from cotton via an efficient route. Carbohydr. Polym. 276, 118766. https://doi.org/10.1016/j.carbpol.2021.118766.

Jarvis, M.C., 2023. Hydrogen bonding and other non-covalent interactions at the surfaces of cellulose microfibrils. Cellulose 30, 667–687. https://doi.org/10.1007/s10570-022-04954-3.

Jiang, L.Q., Fang, Z., Zhao, Z.L., Zheng, A.Q., Wang, X.B., Li, H.B., 2019. Levoglucosan and its hydrolysates via fast pyrolysis of lignocellulose for microbial biofuels: a state-of-the-art review. Renew. Sust. Energ. Rev. 105, 215–229. https://doi.org/10.1016/j.rser.2019.01.055.

Kim, U.J., Eom, S.H., Wada, M., 2010. Thermal decomposition of native cellulose: influence on crystallite size. Polym. Degrad. Stab. 95, 778–781. https://doi.org/10.1016/j.polymdegradstab.2010.02.009.

Koga, N., Vyazovkin, S., Burnham, A.K., Favergeon, L., Muravyev, N.V., Pérez-Maqueda, L.A., Saggese, C., Sánchez-Jiménez, P.E., 2023. ICTAC kinetics committee recommendations for analysis of thermal decomposition kinetics. Thermochim. Acta 719, 179384. https://doi.org/10.1016/j.tca.2022.179384.

Kwon, G.J., Kim, D.Y., Kimura, S., Kuga, S., 2007. Rapid-cooling, continuous-feed pyrolyzer for biomass processing: preparation of levoglucosan from cellulose and starch. J. Anal. Appl. Pyrolysis 80, 1–5. https://doi.org/10.1016/j.jaap.2006.12.012.

Li, M., Wu, K., Yang, K., Chu, C., Wang, S., Yu, J., Zhang, H., 2024. Deconstructing biomass resistance for improving pyrolytic sugars via γ-valerolactone pretreated bamboo coupled with fast pyrolysis. Biomass Bioenergy 181, 107065. https://doi.org/10.1016/j.biombioe.2024.107065.

Li, T., Miao, K., Zhao, Z., Li, Y., Wang, H., Watanabe, A., Teramae, N., Wang, K., 2022. Understanding cellulose pyrolysis under hydrogen atmosphere. Energy Convers. Manag. 254, 115195. https://doi.org/10.1016/j.enconman.2021.115195.

Lin, Y.C., Cho, J., Tompsett, G.A., Westmoreland, P.R., Huber, G.W., 2009. Kinetics and mechanism of cellulose pyrolysis. J. Phys. Chem. C 113, 20097–20107. https://doi.org/10.1021/jp906702p.

Liu, Y., Fu, H., Zhang, W., Liu, H., 2022. Effect of crystalline structure on the catalytic hydrolysis of cellulose in subcritical water. ACS Sustain. Chem. Eng. 10, 5859–5866. https://doi.org/10.1021/acssuschemeng.1c08703.

Lv, Y., Liu, X., Zhou, S., Yu, Q., Xu, Y., 2022. Microbial saccharification–biorefinery platform for lignocellulose. Ind. Crops Prod. 189, 115761. https://doi.org/10.1016/j.indcrop.2022.115761.

Mukarakate, C., Mittal, A., Ciesielski, P.N., Budhi, S., Thompson, L., Iisa, K., Nimlos, M. R., Donohoe, B.S., 2016. Influence of crystal allomorph and crystallinity on the products and behavior of cellulose during fast pyrolysis. ACS Sustain. Chem. Eng. 4, 4662–4674. https://doi.org/10.1021/acssuschemeng.6b00812.

Park, S.Y., Kim, H.L., Her, J.Y., 2024. Isolation of microcrystalline cellulose (MCC) from pistachio shells and preparation of carrageenan-based composite films. Carbohydr. Polym. Technol. Appl. 7, 100423. https://doi.org/10.1016/j.carpta.2024.100423.

Sang, S., Zhuang, X., Chen, H., Qin, Y., Cao, J., Fan, F., Lan, T., 2022. Effect of supramolecular structural changes during the crystalline transformation of cellulose on its enzymatic hydrolysis. Ind. Crops Prod. 180, 114687. https://doi.org/10.1016/j.indcrop.2022.114687.

Segal, L., Creely, J.J., Martin, A.E., Conrad, C.M., 1959. An empirical method for estimating the degree of crystallinity of native cellulose using the X-Ray diffractometer. Text. Res. J. 29, 786–794. https://doi.org/10.1177/004051755902901003.

Silva Filho, E.C., Lima, L.C.B., Silva, F.C., Sousa, K.S., Fonseca, M.G., Santana, S.A.A., 2013. Immobilization of ethylene sulfide in aminated cellulose for removal of the divalent cations. Carbohydr. Polym. 92, 1203–1210. https://doi.org/10.1016/j.carbpol.2012.10.031.

Silveira Junior, E.G., Silveira, Td.C., Perez, V.H., Justo, O.R., David, G.F., Fernandes, S. A., 2022. Fast pyrolysis of elephant grass: intensification of levoglucosan yield and other value-added pyrolytic by-products. J. Energy Inst. 101, 254–264. https://doi.org/10.1016/j.joei.2022.02.003.

So, K.S., Brown, R.C., 1999. Economic analysis of selected lignocellulose-to-ethanol conversion technologies. Appl. Biochem. Biotech. 79, 633–640. https://doi.org/10.1385/ABAB:79:1-3:633.

de Souza, A.G., Junqueira, M.T., de Lima, G.F., Rangari, V.K., Rosa, D.S., 2020. A new proposal of preparation of different polymorphs of nanocellulose from eucalyptus citriodora. J. Polym. Environ. 28, 1150–1159. https://doi.org/10.1007/s10924-020-01672-4.

Uetani, K., Hatori, K., 2017. Thermal conductivity analysis and applications of nanocellulose materials. Sci. Technol. Adv. Mat. 18, 877–892. https://doi.org/10.1080/14686996.2017.1390692.

Verma, J., Petru, M., Goel, S., 2024. Cellulose based materials to accelerate the transition towards sustainability. Ind. Crops Prod. 210, 118078. https://doi.org/10.1016/j.indcrop.2024.118078.

Wada, M., Chanzy, H., Nishiyama, Y., Langan, P., 2004. Cellulose III_I crystal structure and hydrogen bonding by synchrotron X-ray and beutron fiber diffraction. Macromolecules 37, 8548–8555. https://doi.org/10.1021/ma0485585.

Wang, Z., McDonald, A.G., Westerhof, R.J.M., Kersten, S.R.A., Cuba-Torres, C.M., Ha, S., Pecha, B., Garcia-Perez, M., 2013. Effect of cellulose crystallinity on the formation of a liquid intermediate and on product distribution during pyrolysis. J. Anal. Appl. Pyrolysis 100, 56–66. https://doi.org/10.1016/j.jaap.2012.11.017.

Wohlert, M., Benselfelt, T., Wågberg, L., Furó, I., Berglund, L.A., Wohlert, J., 2022. Cellulose and the role of hydrogen bonds: not in charge of everything. Cellulose 29, 1–23. https://doi.org/10.1007/s10570-021-04325-4.

Wu, K., Zha, Z., Yang, K., Wu, H., Chu, C., Li, M., Luo, B., Wang, S., Zhang, H., 2024b. Thermal behavior and production distributions of organosolv-phase oxidization pretreatment of biomass coupled with fast pyrolysis. Energy 291, 130359. https://doi.org/10.1016/j.energy.2024.130359.

Wu, K., Lu, Q., Cao, Q., Dhmees, A.S., Yang, K., Wang, S., Yu, J., Hu, L., Zhang, H., 2024a. Hydrolytic and pyrolytic technologies of pretreatment lignocellulose for production of ethanol fuels-A comparative review. Ind. Crops Prod. 218, 118840. https://doi.org/10.1016/j.indcrop.2024.118840.

Xu, C., Tong, S., Sun, L., Gu, X., 2023. Cellulase immobilization to enhance enzymatic hydrolysis of lignocellulosic biomass: an all-inclusive review. Carbohydr. Polym. 321, 121319. https://doi.org/10.1016/j.carbpol.2023.121319.

Yang, X., Zhao, Y., Li, R., Wu, Y., Yang, M., 2018. A modified kinetic analysis method of cellulose pyrolysis based on TG-FTIR technique. Thermochim. Acta 665, 20–27. https://doi.org/10.1016/j.tca.2018.05.008.

Yoneda, Y., Mereiter, K., Jaeger, C., Brecker, L., Kosma, P., Rosenau, T., French, A., 2008. Van der waals versus hydrogen-bonding forces in a crystalline analog of cellotetraose: cyclohexyl 4′-o-cyclohexyl β-d-cellobioside cyclohexane solvate. J. Am. Chem. Soc. 130, 16678–16690. https://doi.org/10.1021/ja805147t.

Yue, Y., Han, J., Han, G., Zhang, Q., French, A.D., Wu, Q., 2015. Characterization of cellulose I/II hybrid fibers isolated from energycane bagasse during the delignification process: Morphology, crystallinity and percentage estimation. Carbohydr. Polym. 133, 438–447. https://doi.org/10.1016/j.carbpol.2015.07.058.

Zhang, J., Wang, Y., Zhang, L., Zhang, R., Liu, G., Cheng, G., 2014. Understanding changes in cellulose crystalline structure of lignocellulosic biomass during ionic liquid pretreatment by XRD. Bioresour. Technol. 151, 402–405. https://doi.org/10.1016/j.biortech.2013.10.009.

Zhang, Y., Yi Teah, H., Xu, F., Zhou, T., Guo, Z., Jiang, L., 2023. Selective saccharification of crude glycerol pretreated sugarcane bagasse via fast pyrolysis: reaction kinetics and life cycle assessment. Bioresour. Technol. 382, 129166. https://doi.org/10.1016/j.biortech.2023.129166.